PNAS
www.pnas.org

Supplementary Information for

Physical mechanisms of amyloid nucleation on fluid membranes

Johannes Krausser, Tuomas P. J. Knowles and Anđela Šarić

Anđela Šarić.
E-mail: a.saric@ucl.ac.uk

This PDF file includes:

Supporting Information Text

This document includes additional information and results on the simulations carried out in the present study. In particular it includes:

- Overview of interaction in the simulation model
- Remark on nucleation in solution vs membrane-assisted nucleation
- Disregarding nucleation in solution
- Coverage of the membrane surface by s-proteins
- Cluster size distribution of bound s-proteins
- Average area per lipid from Voronoi tesselation
- Cluster size distribution of nucleated β-proteins
- Dependence of nucleation rates on β-protein cluster size
- Details on the free energy profiles
- Additional data for the comparison with experimental results
- Lipid solubility in simulations and experiments

Pair-wise interactions between membrane lipids and proteins

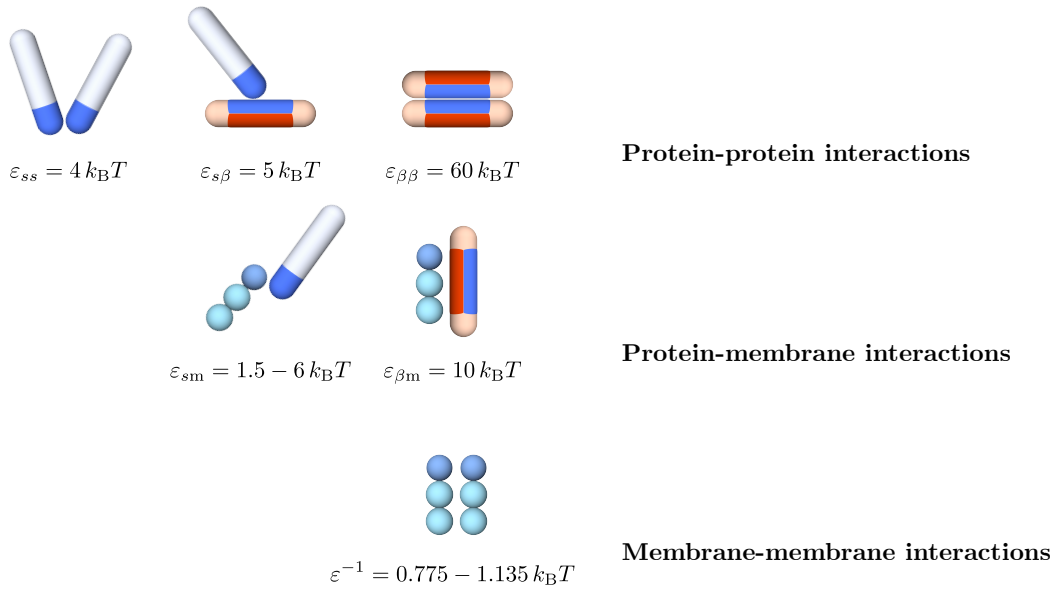

Fig. S1. Overview of interactions in the simulation model: All possible pair interactions between proteins and membranes implemented in the simulation model.

Coverage of the membrane surface by s-proteins

Proteins adsorb to the membrane by virtue of their tip interaction with the lipids which is controlled by the value of $\varepsilon_{s\mathrm{m}}$. Increasing the value of $\varepsilon_{s\mathrm{m}}$ leads to a Langmuir-like behaviour of the membrane coverage θ, as can be seen in Fig. S2(a). Note that due to the fact that the membranes are simulated at zero lateral tension, their area decreases when reducing fluidity due to closer packing of the lipids. The averaging for each value is a configurational and temporal average over 10 realisations and 20 frames separated by 20000 Monte-Carlo time steps each. It is interesting to note that the coverage of the membrane in the gel regime at $k_\mathrm{B}T/\varepsilon = 0.775, 0.815$ is enhanced with respect to the fluid regime. In particular, we can see in Fig. S2(b) that the surface density of bound monomers is significantly higher for membranes of the lowest fluidities with respect to highly fluid membranes. This effect, which increases with higher $\varepsilon_{s\mathrm{m}}$-values, stems from the fact that more ordered membrane

surfaces promote the binding of isolated monomers in the indented pockets of closely packed lipids. This is accompanied by the formation of a brush-like configuration of bound proteins. Figure S2(c) shows the enhancement of bound dimers on the two most gel-like membranes at intermediate membrane-protein affinities ε_{sm} between 3.5 and 4.5 k_BT. This phenomenon also translates to the trimer density, as seen in Fig. S2(d).

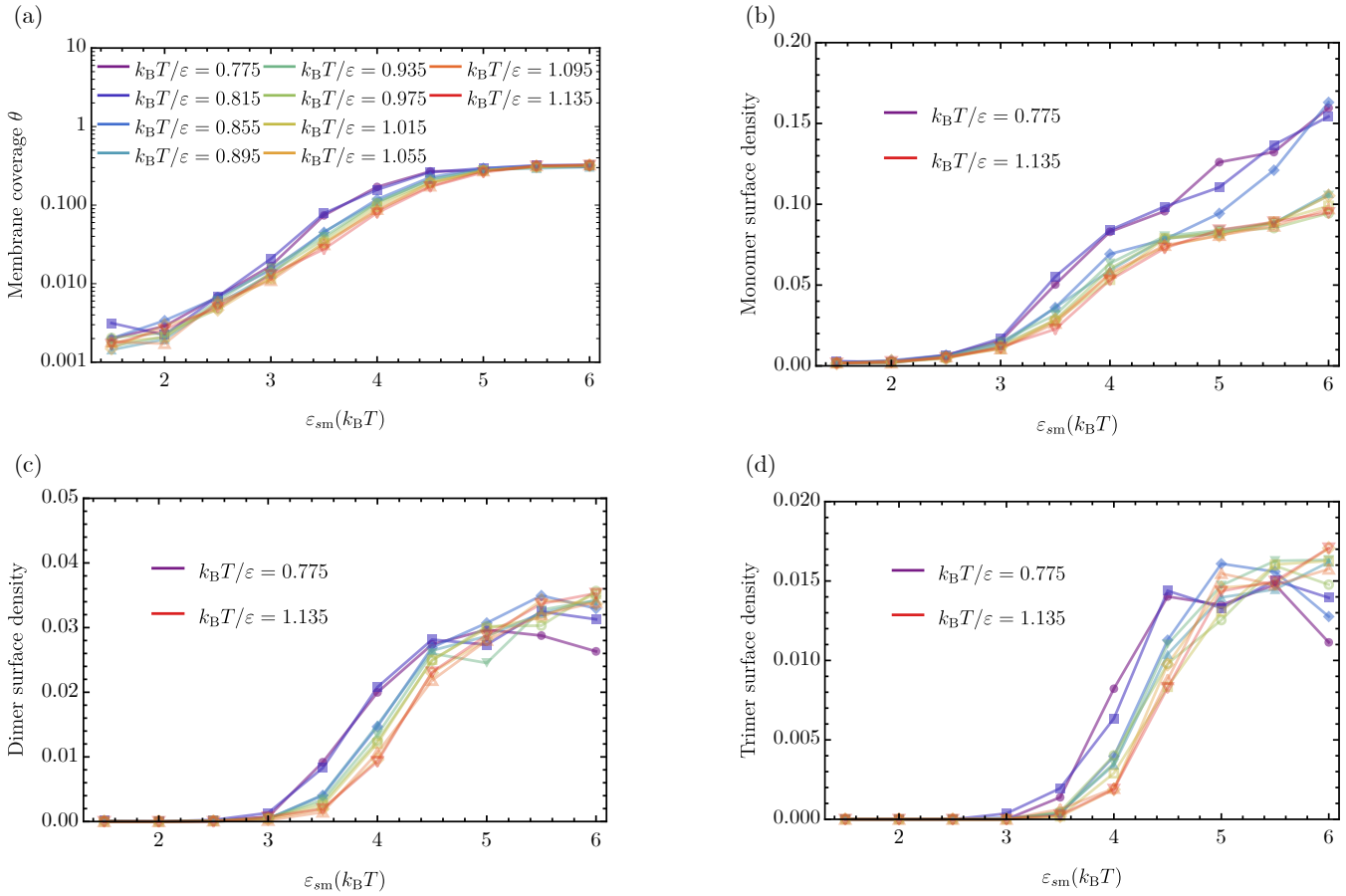

Fig. S2. Membrane coverage characteristics of soluble proteins as a function of ε_{sm} and fluidity: (a) Average number of adsorbed proteins per unit area on the lipid membrane as a function of the protein-membrane fluidity. Different colours indicate ten different values of fluidity in the range $k_BT/\varepsilon \in \{0.775, 0.815, \ldots, 1.135\}$. Average number per unit area of oligomers of increasing size: **(b)** monomers, **(c)** dimers, and **(d)** trimers.

We can understand the behaviour of the membrane coverage in more detail by considering the average cluster size of bound soluble proteins.

Cluster size distribution of bound s-proteins

After equilibration of the Langmuir-like binding isotherm we measured the size distribution of oligomers bound to the membrane. The criterion for two proteins to be counted in the same oligomer is that they must interact through their tips while being bound to the membrane. Note that in this case the oligomer size is obtained before the proteins can switch to their β-sheet forming conformation.

The average cluster size is plotted in Fig. S3(a). It directly derives from the number of bound oligomers up to size 10, as shown in Fig. S2. At the lowest binding affinities the average cluster size can drop below one (only monomers) due to the fact some snapshot during temporal averaging contain no bound proteins. Furthermore, the average cluster size rises more steeply with ε_{sm} for less fluid membranes. Above $\varepsilon_{sm} = 4.5\,k_BT$ the average cluster size for the two least fluid membranes saturates and even drop as ε_{sm} is increased further. This can be explained by the fact that the abundance of bound proteins further drives the lipids in to a close-packed state. There proteins bind strongly in the resulting dents between the close-packed lipid heads which hinders the formation of oligomers and leads to an excess in bound monomers.

Effectively, this results in a opposite scaling of the average cluster size with the fluidity above and below the threshold $\varepsilon_{sm} = 4.5\,k_BT$, which signals a binding regime of strong protein binding. This scaling is shown Fig. S2(b).

Distribution of area per lipid

In order to shed light on the influence of bound protein proteins we computed the distribution of areas per lipids as a function of both the membrane-protein affinity ε_{sm} and the membrane fluidity. The area per lipid distribution was obtained by Voronoi

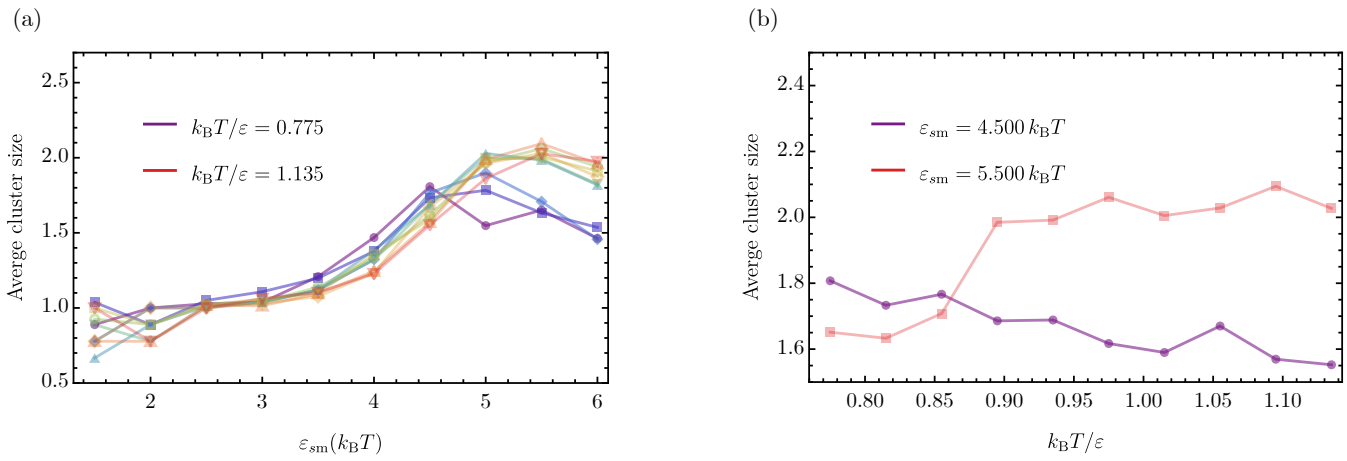

Fig. S3. Average cluster size of bound protein oligomers (a) Average cluster size of soluble protein oligomers bound to the lipid bilayer. Different colours indicate ten different values of fluidity $k_BT/\varepsilon \in \{0.775, 0.815, \ldots, 1.135\}$. **(b)** Slice through **(a)** at the constant protein-membrane affinities $\varepsilon_{sm} = 4.5k_BT$ and $\varepsilon_{sm} = 5.5k_BT$ showing an increase (decrease) of the average oligomer size with growing membrane fluidity.

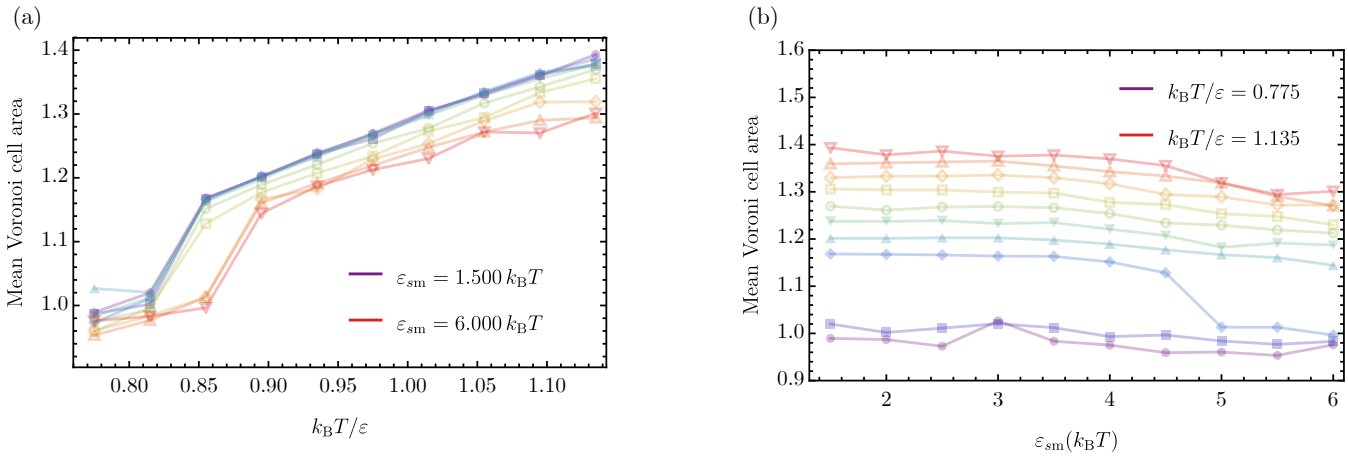

Fig. S4. Average area per lipid: Average area per lipid as a function of **(a)** membrane fluidity and **(b)** membrane-protein affinity obtained via Voronoi tesselation.

tesselation.

Figure S4 shows the average area per lipid as a function of the fluidity. Firstly, we directly can see the signature of the gel-to-fluid membrane phase transition as a jump in the average area per lipid as k_BT/ε is increased, i.e. as the strength of the hydrophobic lipid tail attraction is decreased. In addition we observe that the three cases with the highest membrane-protein affinities exhibit a shifted phase boundary between gel and fluid. The adsorption of proteins delays the gel-fluid transition towards higher k_BT/ε-values. Or put differently, the adsorption of s-proteins to the membrane can induce a fluid-to-gel transition.

Cluster size distribution of bound β-proteins

In addition to the case of soluble proteins, we also recorded the oligomer size distribution of converted β-proteins. Simulations were run until 20 proteins have converted to their β-state, then the cluster size distribution was recorded. Here, the criterion for being counted in the same cluster is that two proteins have to be interacting through their side patches in the β-conformation. The results can be seen in Fig. S5.

The average cluster size of β-prone prone proteins depends on both the membrane-protein affinity ε_{sm} and the membrane fluidity. High membrane-protein affinities entail a high membrane coverage, which in turn leads to the quick elongation of nucleated β-proteins. This manifests itself in a average cluster size of 20 for the lowest fluidity above affinities of $\varepsilon_{sm} = 4.5\,k_BT$.

We can observe that increasing fluidity tends to reduce the average β-cluster size due to the increased tendency towards producing mixed lipid-protein clusters.

Dependence of the nucleation rates on the cluster size

As discussed in the main text, the nucleation rates in Fig. 3 are determined by the time step where the first β-prone dimer is formed. In Fig. S6 we report the dependence of the nucleation rate of clusters on the size of the cluster. The main

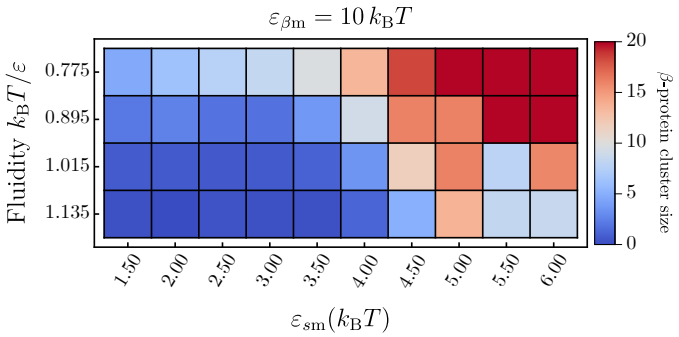

Fig. S5. Average size of β-protein clusters: Average cluster size distribution once 20 β-prone proteins were formed.

conclusion we can draw from this analysis is that the formation of higher order β-clusters is suppressed in the regime of small membrane-protein affinities and high fluidities. This can be explained by the consideration that fast formation of higher order β-cluster on the one hand requires a local environment enriched in bound proteins, which is not provided at low ε_{sm}-values and on the other hand can be inhibited by the absorption of β-proteins into the membrane core facilitated at high fluidities.

Details on the free energy profiles

The potentials of mean force (PMF) for both protein species were obtained using Umbrella simulations in which one isolated protein was brought into interaction with the lipid bilayer by lowering the protein in a stepwise fashion from solution into the the centre of the lipid membrane.

Therefore, these simulations inherently cannot account for cooperative effects between proteins but will only reflect the influence of the membrane on the conversion probability of a single isolated protein.

From the umbrella simulation we obtained the two potentials of mean force for the soluble and β-like protein, denoted by $\mathcal{V}_s = \mathcal{V}_s(z, \varepsilon, \varepsilon_{\mathrm{sm}})$ and $\mathcal{V}_\beta = \mathcal{V}_\beta(z, \varepsilon, \varepsilon_{\beta\mathrm{m}})$, respectively. Here, the variable z designates the centre-of-mass separation between the membrane and the protein.

A single protein is placed at a sufficient distance from the membrane to be out of interaction range. Then the protein is inserted into the membrane using a biasing potential, as illustrated in Fig. 4. Subsequently, the weighted histogram analysis method (1) is used to compute $\mathcal{V}(z)$. The resulting PMFs reflect the corresponding free energy of binding in the protein-membrane system.

We distinguish the free energy profiles for the s- and β-states of the protein that are denoted by $\mathcal{V}_\mathrm{s}(z)$ and $\mathcal{V}_\beta(z)$, respectively. The minimum position $z_{\mathrm{min},s}$ reflects the average equilibrium binding position of the protein along the membrane normal.

Variation with protein-membrane affinity. As the respective affinities are increased, the depth of both the PMFs of the soluble and β-like proteins increase reflecting the stronger binding of the protein to the membrane, as can be seen in Fig. S7(a) and (b) for $k_\mathrm{B}T/\varepsilon = 0.895$. In addition to this, we observe that the minimum of $\mathcal{V}_s$ shifts also in position to lower values of the centre-of-mass separation, which is not the case for $\mathcal{V}_\beta$. This results from the model assumption that soluble proteins can also interact with the two hydrophobic lipid tails.

At the same time the density profile of the membrane lipids is not affected by increasing the affinity. From this we can conclude that the soluble protein insert further into the lipid bilayer as its affinity to the membrane is increased, which is a result of the specific lipid interaction profile we have chosen.

Variation with membrane fluidity. Varying the membrane fluidity, the soluble PMF reacts differently. This situation is plotted in Fig. S7 (c). At the lowest fluidity $k_\mathrm{B}T/\varepsilon = 0.775$, the protein experiences a strong repulsive branch of the PMF, while being bound in a relatively narrow well on top of the lipid membrane. In the more fluid phases the resulting PMF is markedly softer. We observe both a decrease in the depth of the PMF and and shift to lower values of Δz_{cm}. However, in contrast to the constant fluidity case, now the density profile of the membrane is changed as well which results from the thinning of the membrane as its phase state changes from gel to fluid. The average z position of the lipid head in the top leaf of the membrane decreases from $2.4\sigma \pm 0.35\sigma$ to $1.92\sigma \pm 0.64\sigma$ indicating that the membrane thins and at the same time the lipid head experiences higher fluctuations in z. Going across the gel-fluid transition, the minima of the soluble PMF shifts by more than σ which indicates that the shift in the PMF position is a combination of the thinning of the membrane and a higher mobility along the membrane normal due to higher fluidity.

A slightly different situation arises for the β-like protein as shown in Fig. S7(d). If the membrane is in its gel phase, the PMF $\mathcal{V}_\beta(z)$ exhibits a barrier since the β-proteins do not directly bind to the hydrophilic lipid heads. As the fluidity of the membrane is increased, this barrier vanishes and the resulting value of the PMF minimum decreases with higher fluidities.

In summary, the membrane fluidity in our simulation model has a direct effect on the characteristics of the membrane-protein interaction. As can be seen in Fig. S8(a) both the membrane fluidity and the protein-membrane interaction have a significant effect on the position of the PMF minima for the soluble protein. The resulting affinity is shown in Fig. S8(b). We see that at

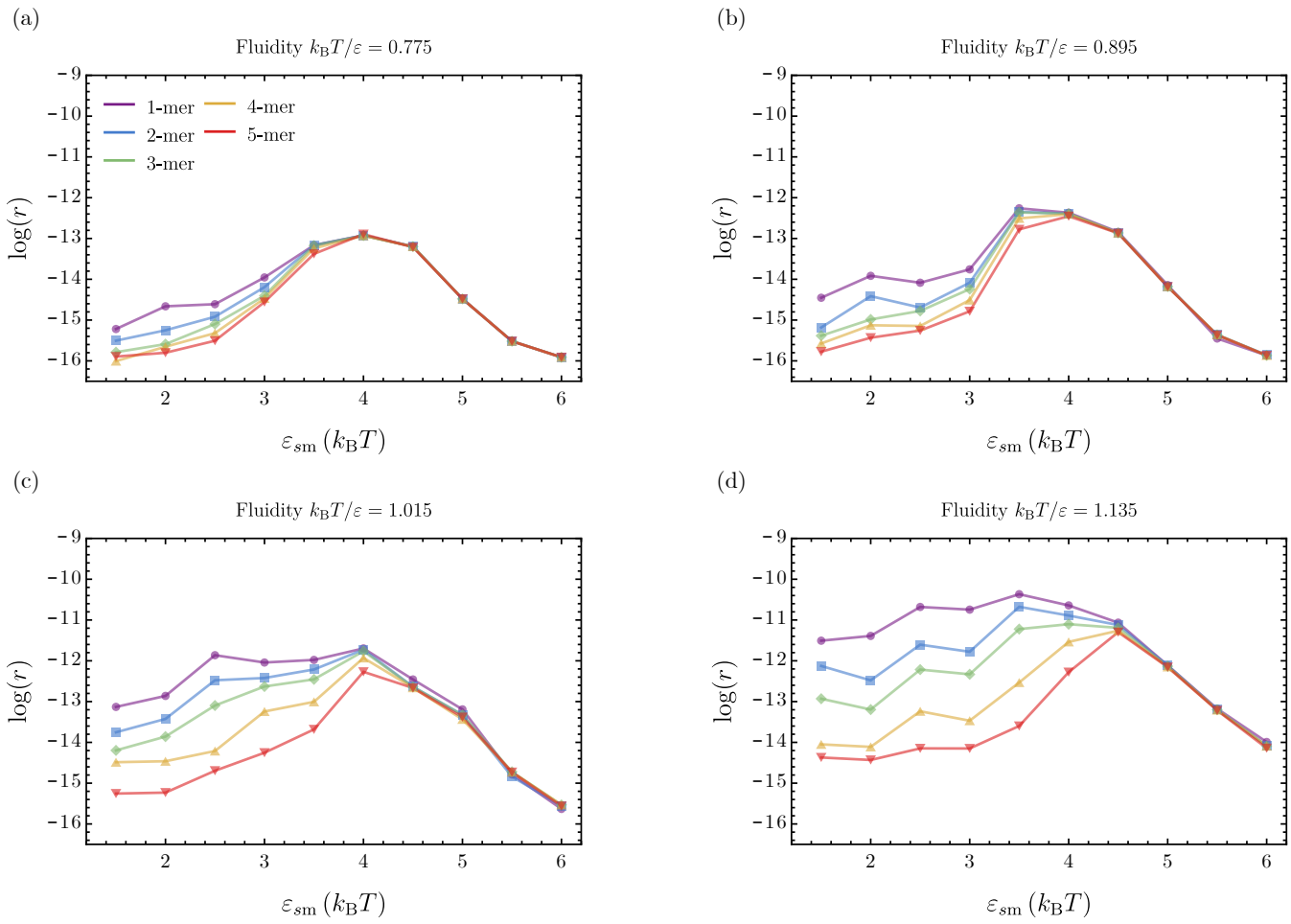

Fig. S6. Nucleation rate for different cluster sizes. The four panels show the nucleation rates as a function of ε_{sm} for the four different fluidities studied in this work. Each panel reports the rate for forming a β-monomer up to a β-pentamer as the membrane fluidity k_BT/ε and the membrane-protein affinity ε_{sm} are varied.

high affinities, the protein is more strongly bound at low fluidities than at high fluidities. This results from the closer packing of the lipid head, and bound protein can arrange in the resulting lattice-like surface of the membrane surface maximising its binding energy.

Comparison of simulation results with experimental data

In order to allow for a quantitative comparison to available experimental data we consider the variation of amyloid nucleation rates as a function of the average area per lipid. Specifically, we consider the relative increase in rates and area per lipid between different fluid membranes with respect to a gel membrane given by $r_{\rm fluid}/r_{\rm gel}$ and $A_{\rm fluid}/A_{\rm gel}$, respectively.

Plotting $r_{\rm fluid}/r_{\rm gel}$ against $A_{\rm fluid}/A_{\rm gel}$ for the two cases discussed in the main text (Fig. 3), we can observe a markedly different scaling. If $\varepsilon_{\beta\rm m} = 0\,k_BT$, $r_{\rm fluid}/r_{\rm gel}$ shows a very weak dependence on the increase in area per lipid, which is cause by increasing membrane fluidity. In contrast to this the interacting case $\varepsilon_{\beta\rm m} = 0\,k_BT$ exhibits a significantly higher variation with the increase in area per lipid caused by the increased exposure of hydrophobic content through membrane defects as fluidity grows. To quantify the different scalings we fitted the two data sets which provides us with two exponents λ for the fitting function of the form

$$r_{\rm fluid}/r_{\rm gel} \propto (A_{\rm fluid}/A_{\rm gel})^{\lambda}\,. \qquad [1]$$

The fits result in $\lambda = 0.42$ for the case $\varepsilon_{\beta\rm m} = 0\,k_BT$ and $\lambda = 14.2$ for the case $\varepsilon_{\beta\rm m} = 10\,k_BT$, as illustrated in Fig. S9.

Lipid solubility in simulations and experiments

Experiments in Ref. (2) have shown that decreases the length of the acyl chain of saturated lipids from $(16:0)_2$ (DPPS) to $(14:0)_2$ (DMPS) and $(12:0)_2$ (DLPS) increases to solubility (or free energy of transfer) ΔG from approximately $-55 kJ\text{mol}^{-1}$ to $-48 kJ\text{mol}^{-1}$ and $-41 kJ\text{mol}^{-1}$, respectively. Under the experimental condition in this Reference, the $(16:0)_2$ lipid vesicles are in the gel phase, whereas the other two are in the fluid phase.

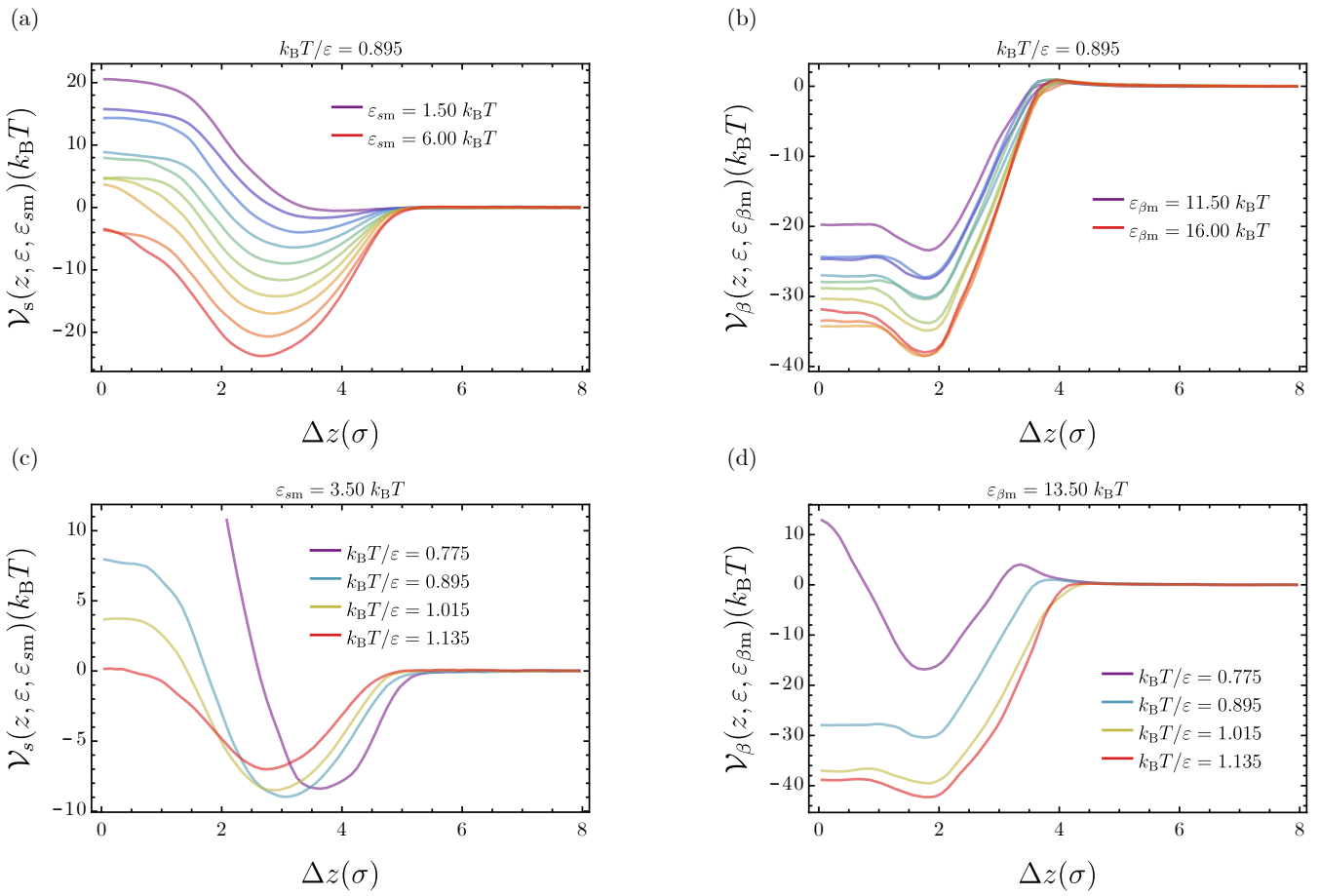

Fig. S7. Free energy profiles of the soluble and β-like protein. The four panels show a selection of free energy profiles: **(a)**, **(b)** at fixed fluidity and **(c)**, **(d)** at fixed affinity. **(a)** Free energy profile of the soluble protein at fixed fluidity $k_BT/\varepsilon = 0.895$ and varying affinities ε_{sm}. **(b)** Free energy profile of the β-like protein at fixed fluidity $k_BT/\varepsilon = 0.895$ and varying affinities $\varepsilon_{\beta m}$. **(c)** Free energy profile of the soluble protein at fixed affinity $\varepsilon_{sm} = 3.50 k_BT$ and varying fluidity. **(d)** Free energy profile of the β-like protein at fixed affinity $\varepsilon_{\beta m} = 13.50 k_BT$ and varying fluidity.

The corresponding values of the lipid free energy of transfer in our simulations exhibit the same trend when reducing the interaction strengths between the lipid tails (i.e. going from the gel to the lipid phase). However, a precise match of the numerical values of the lipid solubility cannot be achieved from such a general lipid membrane model.

For the different fluidities $k_BT/\varepsilon = 0.775, 0.895, 1.015$ and 1.135 the value of the lipid solubility in simulations is approximately $\Delta G = -45 kJ\text{mol}^{-1}, -35 kJ\text{mol}^{-1}, -25 kJ\text{mol}^{-1}$ and $-15 kJ\text{mol}^{-1}$, respectively.

Remark on nucleation in solution vs membrane-assisted nucleation

We have confirmed that for a conversion free energy barrier of $\Delta F_{s\to\beta} = 20\, k_BT$ nucleation in solution never occurs within our simulation time ($4 * 10^7$ Monte-Carlo time steps). This is the case using the protein number concentration of 0.002, a protein self-interaction $\varepsilon_{ss} = 4\, k_BT$ and a switching attempt frequency of 100, the same conditions used in the simulations in the presence of the lipid bilayer. Under these condition, with a β-membrane interaction $\varepsilon_{\beta m} = 20 k_BT$ nucleation occurs on average after $1.2 * 10^5$ time steps in the presence of a fluid membrane ($k_BT/\varepsilon = 1.015$) in intermediate the protein-membrane affinity regime at $\varepsilon_{sm} = 3.5\, k_BT$. Hence, membrane-assisted nucleation in our model can be significantly faster than homogeneous nucleation, as reported experimentally.

Even though our model is simple, the large number of lipids and the need for a substantial nucleation statistics prevents us from exploring slow nucleation mechanisms, which is needed to be able to understand the requirements for fast nucleation. To be able explore the slow nucleation mechanisms realised in the case of a gel-like membrane and at both high and low values of protein-membrane affinity ε_{sm} we reduced the conversion free energy barrier to $\Delta F_{s\to\beta} = 10\, k_BT$ in all our simulations. At the same time the β-membrane interaction was scaled proportionally to $\varepsilon_{\beta m} = 10\, k_BT$. This does not change the nucleation mechanism, but renders it substantially faster to make it computationally accessible. In addition a condition was imposed that $s \to \beta$ conversion can occur only in the presence of a lipid molecule, to prevent possible nucleation in solution that can occur for this lowered barrier but does not occur for $\Delta F_{s\to\beta} = 20\, k_BT$ and $\varepsilon_{\beta m} = 10\, k_BT$ and does not occur in experiments (see also the section "Disregarding nucleation in solution" below).

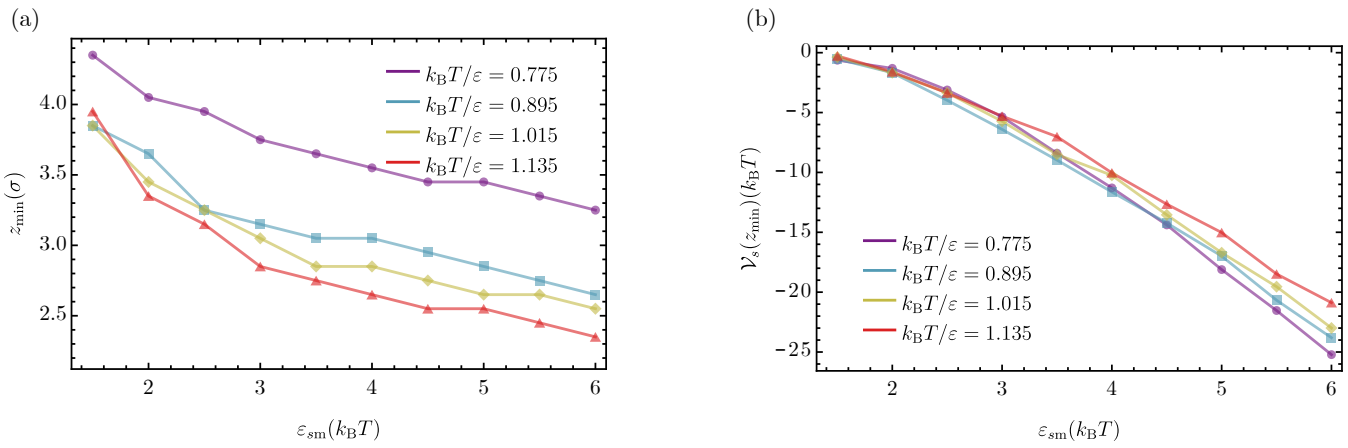

Fig. S8. Minima of the soluble potential of mean force: (a) Position of the minima of $\mathcal{V}_s(z)$ as a function of ε_{sm}. Different colours indicate the four different membrane fluidities discussed in this work. (b) Depth of the free energy profile $\mathcal{V}_s(z)$ at the minimum position z_{min} as a function of membrane fluidity and membrane-protein affinity.

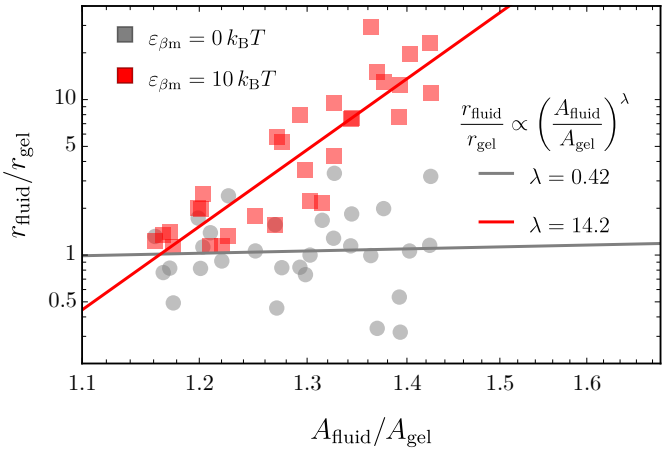

Fig. S9. Increase in nucleation rates as a function of area per lipid: The relative increase in nucleation rates is plotted against the relative increase in area per lipid for the two cases with and without interactions between the lipid tails in the β-prone proteins. In addition, fits to the data points are shown to retrieve the scaling exponent λ.

Imposing this scheme allows us to efficiently sample the full range of parameters in our simulation. In particular, the full range of protein-membrane affinities ε_{sm} up to saturation and the complete gel-to-fluid transition of the lipid bilayer.

Disregarding nucleation in solution

Our focus on surface-driven nucleation is justified by the strong evidence that the nucleation of α-synuclein in the presence of lipid bilayers, which is the physiologically relevant regime, is initiated at the membrane surface and not in solution (3, 4) . Three equally strong pieces of evidence to that end are as follows:

1. In Ref. (4), showed that amyloid nucleation strongly depends on the lipid concentration when vesicles are present in the system. Since such a system is necessarily above CMC, and any added lipid amount goes to the bilayer instead of remaining in the solution, which shows that the nucleation depends on the concentration of bilayer surface, not the concentration of lipids in solution.

2. Using global fitting of experimental kinetic data to an analytical model, which accounts for the key microscopic steps in the aggregation process, Galvagnion et el. (4) determined that the primary nucleation of α-synuclein in the presence of lipid vesicles depends very weakly on the concentration of free monomers in solution. Therefore, free monomers in solution are not directly involved in the rate-determining step in nucleation, and the nucleation does not occur in solution. The same has been shown for Aβ amyloid aggregation as well by Habchi et al. (5).

3. TEM and AFM images have shown fibrils growing between the vesicles (2), as well as from the surface of vesicles (6). If the fibrils were to nucleate in solution it would be very unlikely to acquire such an organisation on the membrane.

Because of this we prevented nucleation in solution and allowed $s \rightarrow \beta$ conformational conversion only in the presence of a lipid.

At higher fluidities and higher solubilities, occasional escape of lipids from the bilayer structure becomes more prevalent. Adding proteins in the soluble state has the effect of stabilising the bilayer structure and reduce lipid escape from the membrane. In the case of very high membrane fluidities, lipid escape however still may happen and interactions between lipids tails and proteins in solution could drive nucleation events. However, we have not recorded these events in our simulations since we intended to isolate the effect of the assembled bilayer on the nucleation kinetics and hence count only the nucleation effects that occur below the distance of 8σ above the equilibrated membrane centre. To check that our approximation is correct, we measured the rate when events on single free lipids in solution are counted (they are events which do not occur at $\Delta F_{s\to\beta} = 20\,k_BT$ but may appear at $\Delta F_{s\to\beta} = 10\,k_BT$) and compared it to the rate when only nucleation on the membrane surface is considered. This is shown in Fig. S10 for the highest fluidity $k_BT/\varepsilon = 1.135$ and it is evident that this only leads to a minimal difference in the overall nucleation kinetics. At lower fluidities no difference in nucleation rates appears in our simulations.

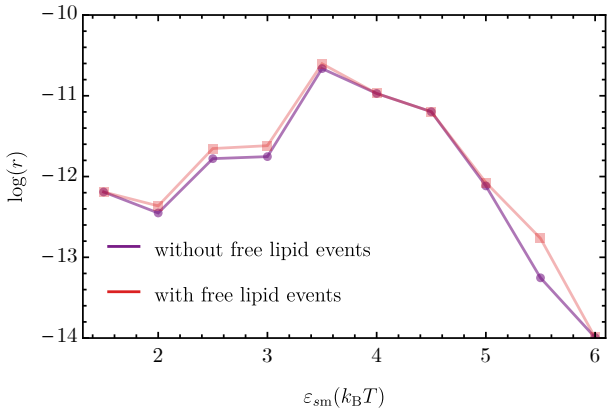

Fig. S10. Contribution of free lipid nucleation events Nucleation rates of dimers were measured at different membrane-protein affinities at $k_BT/\varepsilon = 1.135$. The curve in purple contains only events on the membrane surface and the red curve also contains events on free lipids in solution.

References

1. J Kästner, Umbrella sampling. *Wiley Interdiscip. Rev. Comput. Mol. Sci.* **1**, 932–942 (2011).
2. C Galvagnion, et al., Chemical properties of lipids strongly affect the kinetics of the membrane-induced aggregation of α-synuclein. *Proc. Natl. Acad. Sci.* **113**, 7065–7070 (2016).
3. G Fusco, et al., Direct observation of the three regions in α-synuclein that determine its membrane-bound behaviour. *Nat. Commun.* **5**, 1–8 (2014).
4. C Galvagnion, et al., Lipid vesicles trigger α-synuclein aggregation by stimulating primary nucleation. *Nat. Chem. Biol.* **11**, 229–234 (2015).
5. J Habchi, et al., Cholesterol catalyses Aβ42 aggregation through a heterogeneous nucleation pathway in the presence of lipid membranes. *Nat. Chem.* **10**, 673–683 (2018).
6. JH Lee, et al., Radiating Amyloid Fibril Formation on the Surface of Lipid Membranes through Unit-Assembly of Oligomeric Species of α-Synuclein. *PLoS ONE* (2012).